IEEE Access
Multidisciplinary | Rapid Review | Open Access Journal

Received July 14, 2019, accepted July 28, 2019, date of publication July 30, 2019, date of current version August 16, 2019.

Digital Object Identifier 10.1109/ACCESS.2019.2932094

New Results for Battery Impedance at Very Low Frequencies

JONATHAN SCOTT, (Senior Member, IEEE), AND RAHAT HASAN, (Student Member, IEEE)
School of Engineering, The University of Waikato, Hamilton, New Zealand

Corresponding author: Rahat Hasan (rh163@students.waikato.ac.nz)

This work was supported in part by the Intelligent Tek Limited, and in part by the WaikatoLink Limited.

ABSTRACT In search of an equivalent circuit model for rechargeable batteries, many authors start with a measurement of battery impedance, spanning what is presumed to be the frequency range of interest. Various networks have been suggested in the literature to account for the measured impedance characteristic. Most incorporate two or more resistors, at least one capacitor, some include at least one Warburg element, and more recently ''constant phase elements'' (CPE), otherwise identified as fractional-derivative capacitors. Networks that are more successful at reproducing the measured impedance have from five up to tens of degrees of freedom. The frequency range upon which most models are based extends only to 1mHz. This is surprising since many batteries see a daily or longer usage cycle, corresponding to a frequency of $\approx 11.6\ \mu$Hz or lower. We show in this manuscript that the most-cited impedance measurement instrument, and one of the few that can operate below 1mHz, can be unreliable at and below this boundary. We present a novel impedance measurement algorithm robust against the issues present while measuring the impedance of electrochemical systems to as low as 1 μHz. Next, we present reliable impedance data extending to a lower frequency limit of 10 μHz. A remarkable characteristic appears at the lower frequencies, suggesting a surprisingly simple and elegant equivalent circuit consisting of a single fractional capacitor. A new model is proposed, which requires only four parameters to predict the measured impedance as a function of frequency.

INDEX TERMS Equivalent circuit model, frequency domain analysis, impedance measurement, rechargeable batteries.

I. INTRODUCTION

A great many manuscripts appear in the literature describing rechargeable battery equivalent-circuit models of widely-varying complexity. Some 100 papers have been published in IEEE journals in the last 6 years alone with the words ''battery model'' and ''equivalent circuit'' in the title, with a commensurately larger number of conference manuscripts appearing. Researchers sometimes use time-domain I/V data to which to fit their model, but most carry out an Electro-Impedance Spectroscopy (EIS) measurement, yielding the complex impedance as a function of frequency. The challenge is then to select a circuit topology that is as simple as possible, yet fits the impedance data reasonably well.

A circuit battery model is considered key to prediction of behaviour, including state-of-charge (SoC) and state-of-health (SoH). [1], [2] Most commonly-appearing models are Thévenin-like RC models based around a voltage source [1], [3]–[6] In particular [6] sets the scene well and provides a very comprehensive equivalent circuit, but one requiring a lot of parameters. In [7] an arbitrary number of RC networks are considered, while [8] provides tables of sensitivities of model performance to various parameters, exemplifying the tendency towards ever-increasing complexity. In contrast, [9] trades complexity for speed, potentially using only 3 resistors and 2 capacitors in the model of series impedance.

More recently, researchers have returned to the idea that batteries have fractional characteristics, first noted by Randles in 1947 [10]. The authors have adapted Swingler's method as described in [11] to confirm that rechargeable batteries are fractional in nature and thus not readily accounted for by any finite, compact, equivalent-circuit model [12]. Various manuscripts present models that include fractional characteristics. For example, [13] and [14] approach the problem mathematically rather than through an equivalent circuit, while [15] presents an equivalent-circuit model incorporating both a fractional capacitor, and a Warburg element

The associate editor coordinating the review of this manuscript and approving it for publication was Xiaosong Hu.

(a fractional capacitor of fixed order equal to 0.5, as employed by Randles).

References [13], [14], [16]–[21] all discuss fitting models to batteries using impedance data starting at frequencies of 1mHz, 2mHz, and higher. Many references are not specific about their frequency range, and present only Nyquist, not Bode plots. This is surprising, since many batteries are in appliances charged daily, corresponding to a frequency of $\approx$11.6μHz. Reference [22], now over 20 years old, appears to be alone in arguing that data down to 1μHz may be useful, but even this manuscript presents data down to only 6.8μHz, and there is no discussion of how this data was obtained. In many manuscripts the instrument used to obtain impedance measurement is not stated. We are left to speculate about the reasons for this choice of frequencies.

It may be as simple a reason as convenience. Various manufacturers make instruments that can measure complex impedance to low frequencies, such as the Solartron 1260A Impedance/Gain-Phase Analyzer [23], Chemical Impedance Analyzer IM3590 [24] and MFIA 500 kHz Impedance Analyzer [25]. Most of the available instruments do not go below 1mHz. The instrument in [23], Solartron 1260A, boasts the lowest available frequency of operation of any commercial instrument we could find, 10μHz. This instrument is specifically mentioned in several manuscripts, e.g. [21], [26], [27], and appears to be a popular choice for battery measurements, at which it is specifically targeted by its makers.

II. BATTERY IMPEDANCE MEASUREMENT

Using Solartron 1260A we measured first a single 55123 1850mAh NiMH battery. The cell was set to about 60% state-of-charge (SoC) and allowed to stabilise. The cell was maintained at an ambient temperature of 25 Celcius using a Contherm Polar 1000. We then measured a back-to-back pair, connected in anti-parallel so as to cancel out their dc voltages. The results appear in figure 1.

Confused by the lack of agreement between the two traces, we repeated a measurement of the impedance of the single original cell at 1mHz a number of times using Solartron 1260A. In eight sequential measurements we obtained values varying randomly between 0.59Ω and 0.72Ω. It is obvious that factors beyond the user's control affect the measured impedance. We then measured a 100μF capacitor from 1Hz to 10μHz and obtained the correct result with the stated accuracy for the machine. In other words, a standard electronic component would be measured correctly, but a battery gave results that were not repeatable. Attempts to measure the impedance of human-implantable electrodes using the same instrument, a case where the correct answer is known [28], [29], were similarly unsuccessful [30].

In order to discover whether it was the "wet" device, our use of the instrument, or a shortcoming of the instrument itself, we devise a more rigorous measurement method. The intention is to measure impedance using a programmable current source that is reprogrammed moment by moment to produce a sine-varying current, and frequency by frequency

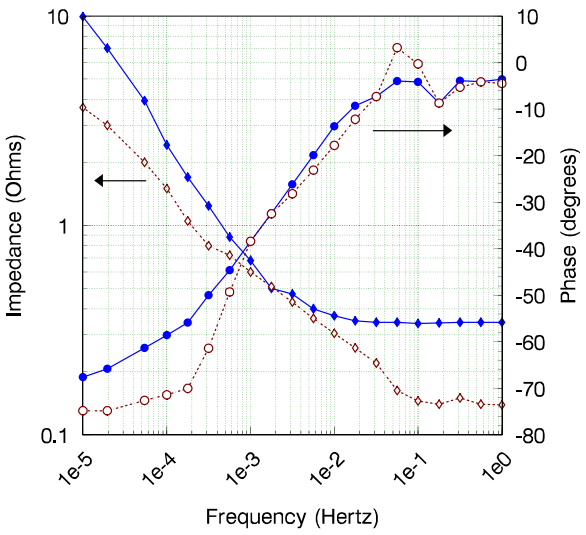

FIGURE 1. Impedance magnitude (diamonds) and phase (dots) of a single 55123 NiMH battery (solid lines) and half the impedance of a back-to-back pair (dashed lines) measured using the impedance analyser of [23].

to adjust the stimulus level. This will ensure that zero net charge is transferred in each cycle of the stimulus. The stimulus level needs to be adjusted, since "small signal" in the case of a battery is the size of the charge inserted in positive half cycles of the stimulus and removed in the negative half cycles. Assume the signal has an amplitude of I_0 and frequency f. The time domain equation of the signal is

$$I = I_0 sin(2\pi ft) \tag{1}$$

The integral of current will yield the amount of charge transferred to and from the cell. The area under the positive half cycle is the amount of charge moved into the cell, Q_{in} and the negative half of the cycle represents the amount of charge moved out of the cell, Q_{out}:

$$Q_{in} = \int_0^{T/2} Idt = \int_0^{T/2} I_0 sin(2\pi ft)dt \tag{2}$$

and

$$Q_{out} = \int_{T/2}^{T} Idt = \int_{T/2}^{T} I_0 sin(2\pi ft)dt \tag{3}$$

Integration of (2) and (3) produces

$$Q_{in} = -\frac{I_0}{2\pi f}[cos(2\pi ft)]_0^{T/2} = -\frac{I_0}{2\pi f}[cos(\pi fT) - 1] \tag{4}$$

and similarly

$$Q_{out} = -\frac{I_0}{2\pi f}[cos(2\pi fT) - cos(\pi fT)] \tag{5}$$

but $fT = 1$ leading to the simple results

$$Q_{in} = \frac{I_0}{\pi f} \tag{6}$$

and

$$Q_{out} = -\frac{I_0}{\pi f} \tag{7}$$

The negative sign denotes the direction of the charge flow with respect to the source. Of course the charge flow over one complete cycle, $\Delta Q = 0$. In situations where ΔQ does not equal zero, there may be unexpected waveform distortion. Observe that the peak amplitude of the charge delivered is dependent on the frequency of the signal. As the frequency of the signal gets smaller and smaller, the current stimulus must be dropped dramatically to prevent the charge excursion flattening or overcharging the DUT (Device Under Test). In our experience, it is prudent to limit charge flow at ± 10 % of the available charge or less in order to stay away from the sharp non-linearities that arise at either end of the charge/discharge characteristic. Much less is better. For low frequencies, low current stimuli must be used, often so low that noise is a major consideration in the measurement. It is worth noting that no instrument we have investigated permits alteration of the stimulus level during an automated sweep. Furthermore, no authors citing measurements discuss the frequency-dependence of what constitutes a "small-signal" measurement.

A range of instruments are able to achieve such a measurement, for example Hameg HM8143 two-quadrant power supplies, Tektronix (Keithley) 2400-series Source-Measurement Units (SMUs), Keysight Precision I/V Analyzers, and Chroma 17000-series Programmable Battery Charge/Discharge Test Systems. The procedure is as follows.

1) Use current drive for the test stimulus signal if possible. This makes it easy to ensure that equal charge is delivered in the positive and negative half sine waves.
2) Before each test frequency, the SoC of the DUT is preset, and the cell rested by fixing the drive voltage corresponding to the required SoC and allowing the cell current to fall to a low value.
3) Fix the amplitude of the stimulus at each new frequency in accordance with equations (6) and (7) and below the maximum safe current level of the DUT.
4) Generate the sinusoidal current waveform at each required frequency.
5) Carry out the measurement over several cycles. Multiple cycles makes Fourier post-processing easier, and can reveal inconsistencies in the time-domain data as the measurement progresses.
6) Store the current and voltage values in a data file for possible diagnostic analysis, as suggested in the last point.
7) Apply a suitable window to the data to account for any signal drift, and extract the magnitude and phase of current and voltage using a Discrete Fourier Transform (DFT) calculated at the stimulus frequency. A suitable DFT algorithm [31] can be computed progressively, and can simultaneously allow for irregular spacing in time of the samples. We use a Hann window.

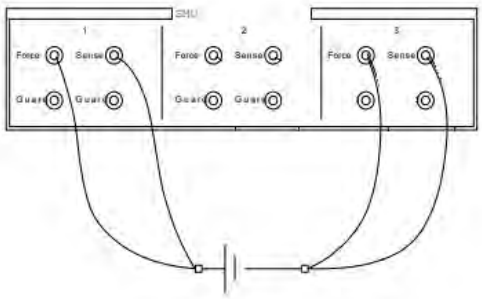

FIGURE 2. Connection to E5270 instrument to measure impedance.

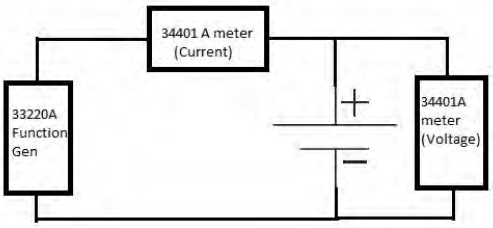

FIGURE 3. The set-up used to measure impedance of NiMH cell using Keysight 33220A Function / Arbitrary Waveform Generator and two 34401A digital multimeters.

8) Calculate the complex impedance by taking the quotient of the voltage and current at the stimulus frequency.

This method is superior because it can produce a signal with arbitrarily low frequency and the post-processing of the IV data is immune to offset drifts, imperfect waveshape, and distortions by virtue of the windowing and filtering.

We repeated the impedance measurement of the same single NiMH cell with our proposed method. Initially, one of us (Hasan) used an Agilent E5270A Precision IV Analyzer with E5281A source/monitor units (SMUs) to achieve this. The connection is shown in Figure 2. The SMU was programmed with a python script. The software communicates with the instrument using the SCPI programming language. For valid comparison between methods, we used the same rested SoC level as before. Throughout the measurement, we kept the external temperature of the cell constant as before. At each frequency, we continued the signal for 6 cycles. All current and corresponding voltage points were saved. Since we had no theoretical expectation with which to compare this result, we decided to confirm it by implementing the same algorithm with code written by a different person (Scott) in a different language (C) on different hardware (Hameg 2-quadrant supply, Agilent DMM). The set-up is shown in Figure 3. The outcomes of these measurements are presented in Figure 4. Our two measurements agreed.

We next used our proposed method to measure the impedance of an 800mAh, 14500 lithium battery. We maintained the external temperature of the cell at 25 degrees Celsius. The measurements were done at 62%

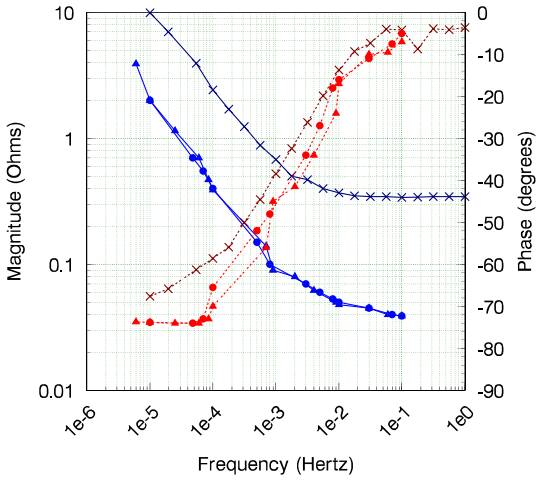

FIGURE 4. Magnitude (left vertical axis, blue traces) and phase (right axis) of the NiMH cell using an SMU (lines with triangle symbols) and a function generator and DMMs (lines with dots) compared with data measured using the commercial impedance analyser (lines with multiplication symbols).

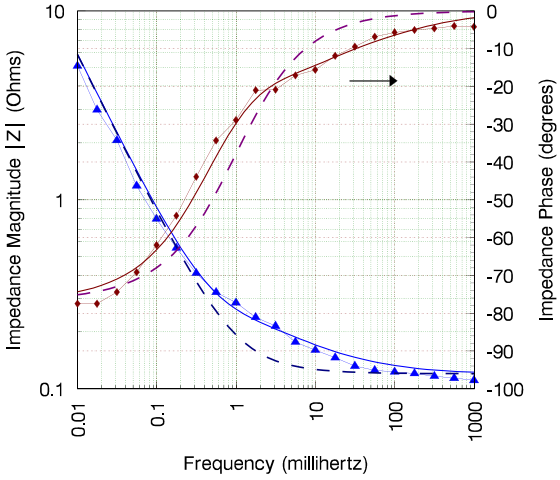

FIGURE 5. Impedance magnitude (left vertical axis, blue traces) and phase (right axis, grey traces) of a 14500 Lithium-ion battery for frequencies starting at 10μHz. Measured data (lines with symbols) compared with the simple R-CPE mathematical model of figure 9 (dashed lines) simulated in Matlab and the split-CPE model of figure 10 (solid lines) simulated in Spice.

State-of-Charge (SoC), although the results do not vary greatly with SoC in the near-linear, middle region. We chose the stimulus level so that the cell SoC does not fluctuate by more than 10% even at 10μHz, where the period of a sinewave is about 27 hours, somewhat more than 1 day, and the test signal can easily overcharge or discharge the battery if chosen too large. The measured values of the magnitude and phase of the impedance of this cell appear in figure 5 (lines with symbols).

III. POSSIBLE REASONS FOR LOW PERFORMANCE

In this section some circumstances that may disturb operation of the Solartron impedance analyser are identified.

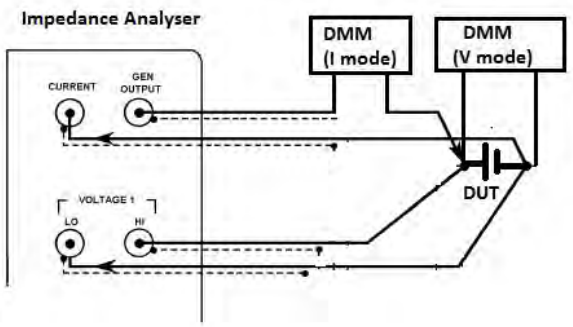

FIGURE 6. Connections to measure the current and voltage during measurement by the impedance analyser.

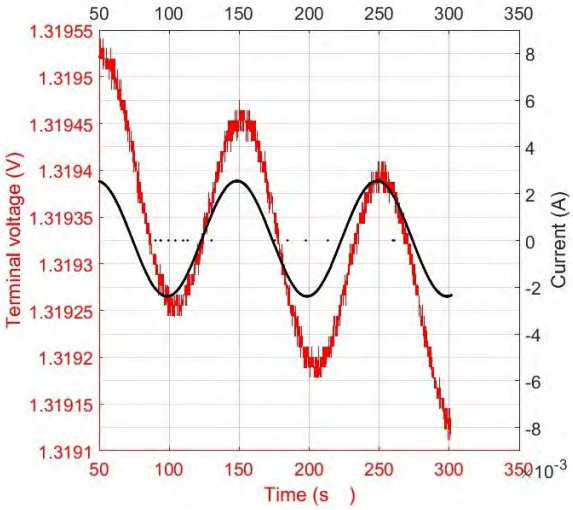

FIGURE 7. Current and voltage measured across the single NiMH cell at 10 mHz.

A. DRIFT IN VOLTAGE WAVEFORM

Curious to understand what causes the impedance analyser to produce erroneous impedance readings when measuring a single cell, we inspected the current and voltage waveforms sourced by the built-in generator. We achieved this by using two Agilent 34401A digital multimeters (DMMs). Figure 6 shows the set-up used to observe the current and voltage responses of the battery. We used identical stimulus level as before. Figure 7 portrays the captured current and voltage waveforms at 10 mHz. Note that the voltage signal is only a few hundred microvolts peak-to-peak, even at 10mHz.

It is clear that there is a downward drift in the voltage waveform measured across the cell, although the current waveform stays sinusoidal. The DC offset of the input signal and the terminal voltage of the battery apparently drifted apart, despite the control of cell temperature.

It may be that the impedance analyser calculates impedance via discrete Fourier Transform. The algorithm of a Fourier Transform assumes that the two endpoints of signals are continuous and there is no discontinuity. Where the endpoints of a signal do not meet, results may be corrupted. This might explain the inaccuracy in impedance measurement. It should also be noted that the analyser carries

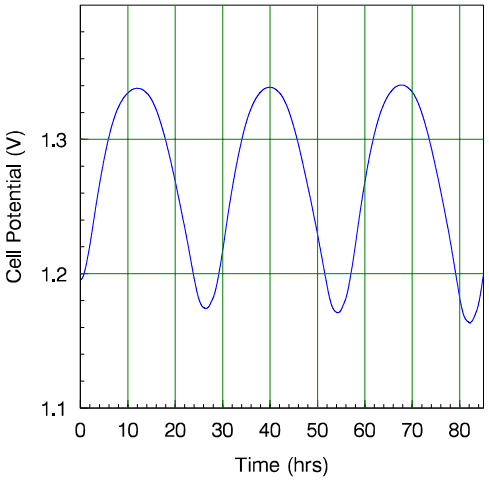

FIGURE 8. Distorted voltage signal observed across a single NiMH cell during measurement at 10 μHz.

out its measurement in one stimulus cycle. This is desirable because of the exceptionally long periods involved. Having only one stimulus cycle makes processes such as windowing data difficult.

B. SIGNAL DISTORTION

Batteries may be close to linear in the mid-range of state-of-charge, typically 40–80%, but are apt to be quite non-linear in the last few percent of their range at both the flat and fully-charged ends of the characteristic. In the case of the NiMH chemistry, trickle-charging is permitted, as there is a mechanism that safely dissipates excess charge delivered as the cell approaches full charge. This mechanism starts to kick in before the last few percent capacity is filled, especially at higher currents. This mechanism can cause the voltage waveform to lose its sinusoidal shape. Figure 8 shows an example voltage signal. This distortion seems to affect our impedance analysers. This reinforces the need to regulate the stimulus magnitude as outlined in section II, as well as to stay away from the ends of the charge curve.

IV. IMPLICATION OF THE IMPEDANCE DATA

A constant phase element/fractional capacitor is an element that obeys the characteristic equation

$$I = C_F \frac{d^\alpha V}{dt^\alpha} \tag{8}$$

which in the Laplace domain is represented by an impedance

$$Z_{C_F} = \frac{-J}{(\omega C_F)^\alpha} \tag{9}$$

giving a straight line on a Bode plot whose slope is not 1 but α, and whose phase is a constant value of $\theta = \pi/2\alpha$, hence the alternate name ''constant phase element''. In the data of figure 5 for example, at lower frequencies where the impedance of the CPE dominates the series pair, the phase settles to a value of $\approx$76 degrees, and the slope of the magnitude trace shows a straight line, but one with slope less than 20dB/decade. The suggested ''R-CPE'' equivalent circuit is

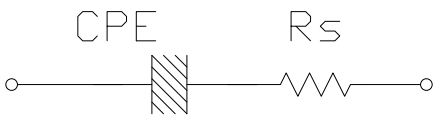

FIGURE 9. Circuit suggested by the asymptotes of the impedance plots.

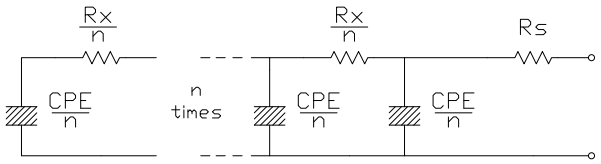

FIGURE 10. Equivalent circuit model with n-way split CPE and series resistance.

shown in figure 9. The pure, Ohmic, series resistance of the battery is $R_S = 0.12\Omega$.

This equivalent circuit was simulated in SPICE using the method outlined in [28] with corrections from [32]. The model parameters are $m = \pi/2\theta_{CPE} = 1.161$ and $Y_\theta = 0.842$ for $\omega_0 = 55.7 \times 10^{-6}$. An accuracy parameter of $k = 1.3$ is found to be more than adequate by trial and error. The simulated impedance from the circuit of figure 9 is shown plotted with the measured data as dashed lines in figure 5. Agreement is good except for the region of the corner frequency.

Recent work described in [33] has shown that allowing for the distributed nature of electrodes by splitting the CPE improves fit in transitional regions. This suggests the equivalent circuit of 10, adding one parameter, R_X. The CPE of the simple model is arbitrarily divided into n smaller CPEs, each of which has the same phase but n times lower an admittance, $Y_{\theta_{split}} = Y_\theta/n$. It remains to discover the value of the $n-1$ resistors R_X present in the split model. The value of R_X has been numerically optimized to obtain the best fit. In this case, we chose a value $R_X = 29\text{m}\Omega$. A 10-way split, that is $n = 10$, was chosen, again by trial and error observing that larger values conferred little advantage. Repeating the simulation of battery impedance with the split-CPE model shows that the new model is more appropriate in the frequency domain. The simulated impedance from the circuit of figure 10 is shown plotted with the measured data as the solid lines in figure 5. Now the fit is excellent.

V. CONCLUSION

We presented impedance measurements on two different batteries extending to very low frequencies. The measurement required the development of a novel algorithm to provide robust, repeatable data. This exposed an exciting characteristic, namely that the impedance data forms a straight line, characteristic of a fractional capacitor, at such very low frequencies. This characteristic has not been observed before.

Based on this impedance characteristic we suggest a new equivalent circuit consisting of a single fractional capacitor or CPE in series with a single resistor. This circuit reproduces the impedance, magnitude and phase, with reasonable

accuracy, using only three parameters. A split-CPE model can reproduce the impedance with greater accuracy. This increases the number of parameters to four.

REFERENCES

[1] G. Nobile, M. Cacciato, G. Scarcella, and G. Scelba, "Performance assessment of equivalent-circuit models for electrochemical energy storage systems," in *Proc. 43rd Annu. Conf. IEEE Ind. Electron. Soc. (IECON)*, Oct./Nov. 2017, pp. 2799–2806.

[2] C. Zhang, K. Li, S. Mcloone, and Z. Yang, "Battery modelling methods for electric vehicles—A review," in *Proc. Eur. Control Conf. (ECC)*, Strasbourg, France, Jun. 2014, pp. 2673–2678.

[3] J. Chiasson and B. Vairamohan, "Estimating the state of charge of a battery," *IEEE Trans. Control Syst. Technol.*, vol. 13, no. 3, pp. 465–470, May 2005.

[4] T. Wu, L. Liu, Q. Xiao, Q. Cao, and X. Wang, "Research on SoC estimation based on second-order RC model," *Telkomnika*, vol. 10, no. 7, pp. 1667–1672, Nov. 2012.

[5] Z. Cheng, J. Lv, Y. Liu, and Z. Yan, "Estimaon of state of charge for lithium-ion battery based on finite difference extended Kalman filter," *J. Appl. Math.*, vol. 2014, Mar. 2014, Art. no. 348537.

[6] M. Chen and G. A. Rincón-Mora, "Accurate electrical battery model capable of predicting runtime and I-V performance," *IEEE Trans. Energy Convers.*, vol. 21, no. 2, pp. 504–511, Jun. 2006.

[7] G. Liu, L. Lu, H. Fu, J. Hua, J. Li, M. Ouyang, Y. Wang, S. Xue, and P. Chen, "A comparative study of equivalent circuit models and enhanced equivalent circuit models of lithium-ion batteries with different model structures," in *Proc. IEEE Conf. Expo Transp. Electrific. Asia–Pacific (ITEC Asia–Pacific)*, Aug./Sep. 2014, pp. 1–6.

[8] A. Seaman, T.-S. Dao, and J. McPhee, "A survey of mathematics-based equivalent-circuit and electrochemical battery models for hybrid and electric vehicle simulation," *J. Power Sour.*, vol. 256, pp. 410–423, Jun. 2014.

[9] A. Fotouhi, D. J. Auger, K. Propp, and S. Longo, "Accuracy versus simplicity in online battery model identification," *IEEE Trans. Syst., Man, Cybern., Syst.*, vol. 48, no. 2, pp. 195–206, Feb. 2018.

[10] J. E. B. Randles, "Kinetics of rapid electrode reactions," *Discussions Faraday Soc.*, vol. 1, pp. 11–19, Mar. 1947.

[11] R. Hasan and J. Scott, "Application of Swingler's method for analysis of multicomponent exponentials with special attention to non-equispaced data," in *Proc. IEEE 12th Int. Colloq. Signal Process. Appl. (CSPA)*, Kuala Lumpur, Malaysia, Mar. 2016, pp. 12–15.

[12] R. Hasan and J. B. Scott, "Fractional behaviour of rechargeable batteries," in *Proc. Electron. New Zealand Conf. (ENZCon)*, Nov. 2016, pp. 111–114. [Online]. Available: https://ecs.victoria.ac.nz/foswiki/pub/Events/ENZCon2016/WebHome/ENZCon2016Proceedings.pdf

[13] M. Cugnet, J. Sabatier, S. Laruelle, S. Grugeon, B. Sahut, A. Oustaloup, and J.-M. Tarascon, "On lead-acid-battery resistance and cranking-capability estimation," *IEEE Trans. Ind. Electron.*, vol. 57, no. 3, pp. 909–917, Mar. 2010.

[14] J. Sabatier, M. Merveillaut, J. M. Francisco, F. Guillemard, and D. Porcelatto, "Fractional models for lithium-ion batteries," in *Proc. Eur. Control Conf. (ECC)*, Zurich, Switzerland, Jul. 2013, pp. 3458–3463.

[15] Y. Ma, X. Zhou, B. Li, and H. Chen, "Fractional modeling and SOC estimation of lithium-ion battery," *IEEE/CAA J. Automatica Sinica*, vol. 3, no. 3, pp. 281–287, Jul. 2016.

[16] B. Saha, K. Goebel, S. Poll, and J. Christophersen, "Prognostics methods for battery health monitoring using a Bayesian framework," *IEEE Trans. Instrum. Meas.*, vol. 58, no. 2, pp. 291–296, Feb. 2009.

[17] D. V. Do, C. Forgez, K. El Kadri Benkara, and G. Friedrich, "Impedance observer for a Li-ion battery using Kalman filter," *IEEE Trans. Veh. Technol.*, vol. 58, no. 8, pp. 3930–3937, Oct. 2009.

[18] H. Chaoui, N. Golbon, I. Hmouz, R. Souissi, and S. Tahar, "Lyapunov-based adaptive state of charge and state of health estimation for lithium-ion batteries," *IEEE Trans. Ind. Electron.*, vol. 62, no. 3, pp. 1610–1618, Mar. 2015.

[19] A. Guha and A. Patra, "Online estimation of the electrochemical impedance spectrum and remaining useful life of lithium-ion batteries," *IEEE Trans. Instrum. Meas.*, vol. 67, no. 8, pp. 1836–1849, Aug. 2018.

[20] A. Carullo, F. Ferraris, M. Parvis, A. Vallan, E. Angelini, and P. Spinelli, "Low-cost electrochemical impedance spectroscopy system for corrosion monitoring of metallic antiquities and works of art," *IEEE Trans. Instrum. Meas.*, vol. 49, no. 2, pp. 371–375, Apr. 2000.

[21] Y.-D. Lee, S.-Y. Park, and S.-B. Han, "Online embedded impedance measurement using high-power battery charger," *IEEE Trans. Ind. Appl.*, vol. 51, no. 1, pp. 498–508, Jan./Feb. 2015.

[22] P. Mauracher and E. Karden, "Dynamic modelling of lead/acid batteries using impedance spectroscopy for parameter identification," *J. Power Sources*, vol. 67, nos. 1–2, pp. 69–84, 1997.

[23] Ametek Scientific Instruments. *Solartron 1260A Impedance/Gain-Phase Analyzer*. Accessed: Jul. 2018. [Online]. Available: https://www.ameteksi.com/products/frequency-response-analyzers/1260a-impedance-analyzer

[24] Hioki E.E. Corporation. (Oct. 2018). *Chemical Impedance Analyzer IM3590, Battery Impedance Meter BT4560*. [Online]. Available: https://www.hioki.com/en/products/detail/?product_key=5749 and https://www.hioki.com/en/products/detail/?product_key=5664

[25] Zurich Instruments. (Oct. 2018). *MFIA 500 kHz Impedance Analyzer*. [Online]. Available: https://www.zhinst.com/products/impedance

[26] Q.-K. Wang, Y.-J. He, J.-N. Shen, X.-S. Hu, and Z.-F. Ma, "State of charge-dependent polynomial equivalent circuit modeling for electrochemical impedance spectroscopy of Lithium-ion batteries," *IEEE Trans. Power Electron.*, vol. 33, no. 10, pp. 8449–8460, Oct. 2018.

[27] G.-A. J. Francisco, R.-G. Juan, G.-C. Manuel, and R.-H. JoséRoberto, "Fractional RC and LC electrical circuits," *Ingeniería, Investigación y Tecnología*, vol. 15, pp. 311–319, Apr./Jun. 2014.

[28] J. Scott and P. Single, "Compact nonlinear model of an implantable electrode array for spinal cord stimulation (SCS)," *IEEE Trans. Biomed. Circuits Syst.*, vol. 8, no. 3, pp. 382–390, Jun. 2014.

[29] M. H. Jones and J. Scott, "Scaling of electrode-electrolyte interface model parameters in phosphate buffered saline," *IEEE Trans. Biomed. Circuits Syst.*, vol. 9, no. 3, pp. 441–448, Jun. 2015.

[30] D. MacCallum, "Automatic measurement of implantable electrode characteristics using a single impedance analyser," M.S. thesis, School Eng., Univ. Waikato, Hamilton, New Zealand, 2017.

[31] J. Scott and A. Parker, "Modern guide to spectral analysis with SPICE," *IEEE Circuits Devices Mag.*, vol. 11, no. 5, pp. 10–16, Sep. 1995.

[32] S. Seshadri and J. Scott, "Correction to 'compact nonlinear model of an implantable electrode array for spinal cord stimulation' [Jun 14 382-390]," *IEEE Trans. Biomed. Circuits Syst.*, vol. 12, no. 4, pp. 963–964, Aug. 2018.

[33] P. Single and J. Scott, "Cause of pulse artefacts inherent to the electrodes of neuromodulation implants," *IEEE Trans. Neural Syst. Rehabil. Eng.*, vol. 26, no. 10, pp. 2078–2083, Oct. 2018.

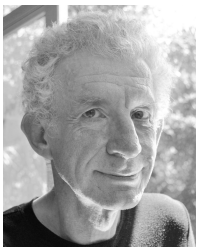

JONATHAN SCOTT (M'80–SM'99) was a Chief Engineer with the RF Technology, Sydney, from 1997 to 1998. From 1998 to 2006, he was with the Hewlett-Packard and Agilent Technologies Microwave Technology Center, Santa Rosa, California, where he was responsible for advanced measurement systems operating from dc to millimeter-wave. He was with the Department of Electrical Engineering, University of Sydney, prior to 1997. He is currently the Foundation Professor of electronic engineering with The University of Waikato, New Zealand. Prof. Scott holds five degrees, has authored over 150 refereed publications, several book chapters and a textbook, and he holds a dozen patents, several covering active products. His research interests include characterization and modeling of implantable electrodes, semiconductor device, battery, and acoustic systems. Professor Scott's educational interest includes Threshold Concepts and their application, particularly across engineering disciplines.

RAHAT HASAN received the B.Eng. degree (Hons.) in electrical and electronic engineering from London South Bank University, U.K. He is currently pursuing the Ph.D. degree with The University of Waikato, New Zealand. From 2011 to 2012, he was with Visteon Engineering Services Ltd, U.K., as a Software Validation Engineer. He is also the CEO and the Co-Founder of Smart Farmer Ltd. and Intelligent Tek Ltd. both of which are working on Agritech Projects.